Boundary-Layer Meteorol (2013) 148:255–268
DOI 10.1007/s10546-013-9819-9

ARTICLE

Turbulent Schmidt Numbers Above a Wheat Crop

J. D. Wilson

Received: 28 October 2012 / Accepted: 21 March 2013 / Published online: 13 April 2013

Abstract Measurements of vertical fluxes and concentration differences above a spring wheat crop (height $h = 0.9$–0.95 m, row spacing 0.25 m, displacement height $d = 0.5$–0.6 m) were analyzed to determine the Schmidt numbers for water vapour (S^{v}) and carbon dioxide (S^{c}) based on concentration differences between intakes 2.55 and 3.54 m above the ground. During nearly-neutral stratification $S^{\mathrm{v}}(0) = 0.68 \pm 0.1$ while $S^{\mathrm{c}} = 0.78 \pm 0.2$, implying that the roughness sublayer extended above $2.5h$.

Keywords Atmospheric surface layer · Eddy diffusivity · Inertial sublayer · Roughness sublayer · Turbulent diffusion · Turbulent Schmidt number

1 Introduction

The turbulent Schmidt number S^{α} is the ratio K/K_{α} of the eddy viscosity K to the eddy diffusivity for a gas species α, these being defined (in the context of a wall shear layer) relative to turbulent transport normal to the boundary. Its value is of secondary interest relative to profiles of the Ks themselves, except that from uncertainty as to its true value it is commonly treated as a prescribed constant, often unity, in a range of environmental models—irrespectively of whether those models address the transport and dispersion of natural species to and from uniform sources (e.g. Glenn et al. 2010), or of artifical species from localized sources (as in air pollution modelling, e.g. Delaunay 1996). Tominaga and Stathopoulos (2007) note that constant values (0.7 or 0.9) "have been set as default in most commercial CFD software."

The prevailing view (e.g. Harman and Finnigan 2008) as regards the value of the generic Schmidt number S for natural tracers in a horizontally homogeneous, neutrally-stratified

J. D. Wilson (✉)
Department of Earth and Atmospheric Sciences, University of Alberta, Edmonton, AB T6G 2E3, Canada
e-mail: jaydee.uu@ualberta.ca

surface layer is that it is approximately 1.0 in the inertial sublayer,[1] but decreases to a value of about 0.5 within the roughness sublayer (RSL) (evidence for this is reviewed in Sect. 2). Both the eddy viscosity and the eddy diffusivity may be enhanced in the RSL, but the increase in the latter prevails so that $S < 1$. The depth of the RSL, if taken to be that layer within which mean vertical gradients are smaller than those anticipated by Monin–Obukhov similarity functions that take into account the displacement height d, has been reported to differ for different properties, and remains quantitatively uncertain (De Ridder 2010). For tall, uniform natural canopies (of height h) Arya (2001) suggests the top of the RSL lies at a distance of about 1.5–2.5h above the ground, while Kaimal and Finnigan (1994) and Foken (2006) suggest 2–3h. We return to this in Sect. 5.

A mechanism definitively explaining the profile of the Schmidt number is elusive, presumably in part because the eddy diffusion paradigm upon which its definition hinges is itself of, at best, conditional validity. Whilst an eddy diffusivity may always be computed from a flux and gradient measured at a given point, it is not in general a property of the turbulent velocity statistics alone, potentially depending also on the distribution of sources and sinks relative to the observation point (Taylor 1921; Raupach 1987; Wilson 1989; Raupach et al. 1996). Thus it is conceivable that the above understanding for $S(z)$, stemming as it does from observations of the transport of naturally occurring gases (especially water vapour), may be inappropriate for quantifying dispersion from (e.g.) point sources to nearby detection points. And on that note it is striking that the Project Prairie Grass (PPG) measurements of dispersion from a continuous point source are best modelled by ascribing to the tracer gas (SO_2) a neutral Schmidt number $S = 0.6$–0.7 (Wilson 1982; Wilson and Yee 2007) or (in Lagrangian models) a value of the Kolmogorov constant C_0 that corresponds to a Schmidt number in that range (Sawford 2001). As the PPG observation points lay above the RSL, such a small value for the Schmidt number is surprising. This contradiction—between the value of the Schmidt number inferred from observed flux–gradient relationships for natural scalars in the inertial sublayer and the value inferred from tracer dispersion experiments (see also Hassid 1983; Wilson et al. 1984)—is a longstanding puzzle.

2 Previous Measurements of the Schmidt Number

In the inertial sublayer where Monin–Obukhov similarity theory (MOST) applies, the eddy diffusivity for a gas α can be written

$$K_\alpha = \frac{\kappa_\alpha u_* (z-d)}{\phi_\alpha(\zeta)} \tag{1}$$

where κ_α is the von Karman constant for (this) gas, d is the zero-plane displacement, $\zeta = (z-d)/L$ where L is the Obukhov length, and $\phi_\alpha(\zeta)$ is the Monin–Obukhov function. Some authors adopt a single von Karman constant κ for all species and permit $\phi_\alpha(0)$ to differ from unity; others (as here) follow the convention that the ϕ functions take the value unity in the neutral limit, and allow distinct von Karman constants. In the latter case the von Karman constants define a value for the Schmidt number in the neutral limit,

$$S^\alpha(0) = \frac{\kappa}{\kappa_\alpha}. \tag{2}$$

[1] The assumption that $S \approx 1$ is rather common *in general*. For example, reviewing the matter in the context of their own measurements of the Schmidt number in a laboratory free shear layer, Huq and Stewart (2008) regard $S \approx 1$ as being expected "in the absence of density stratification."

According to Harman and Finnigan (2008) "there is no strong evidence that (the Schmidt or Prandtl number) differs significantly from unity" above the roughness sublayer, whereas "the scalar roughness sublayer can be defined as the layer across which (the Schmidt number) varies from its canopy-top value of 0.5 in neutral stability to its MOST value of 1.0 above the RSL."

Surprisingly, rather few micrometeorological experiments offer concrete information on this subject. Let us focus specifically on water vapour (flux–gradient experiments with eddy covariance measurements of the carbon dioxide flux are even rarer). Based on evaporation and drag as measured by a 6.1 m diameter drag-plate lysimeter matched to a grass surface, Pruitt et al. (1973) reported $\kappa = 0.42$ and $\kappa_w = 0.47$, implying $S^{\mathrm{v}}(0) = 0.89$. Analyzing the ITCE 1976 experiment in Australia, which entailed the pooling of several eddy covariance systems as well as lysimeter and drag plates, Francey and Garratt (1981) deduced values for the von Karman constants for (e.g.) momentum or water vapour by plotting $\Delta\overline{u}_{21}/\left(u_* \ln(z_1/z_2)\right)$ or $\Delta\overline{q}_{21}/\left(q_* \ln(z_1/z_2)\right)$ versus $\sqrt{z_1 z_2}/L'$, where $\Delta\overline{u}_{21}$, $\Delta\overline{q}_{21}$ are differences in the mean wind speed and specific humidity between heights (z_2, z_1), $q_* \equiv -\overline{w'q'}/u_*$ is the scale for humidity fluctuations, and

$$L' = \kappa L = \frac{-u_*^3 T_{\mathrm{v}0}}{g\overline{w'T_{\mathrm{v}}'}} \tag{3}$$

is a modified Obukhov length defined without including the (sought for) factor κ. Alternative values for the von Karman constants were extracted by presupposing one or another of the pre-existing curves for the MOST functions $\phi(z/L)$ or $\phi(R_i)$, and for instance with

$$\phi = (1 - 15z/L)^{0.25}, \tag{4}$$

$$\phi_w = (1 - 16z/L)^{0.5}, \tag{5}$$

(Dyer 1974) Francey and Garratt infer $\kappa = 0.38 \pm 0.06$ and $\kappa_w = 0.42 \pm 0.06$ (broadly similar outcomes follow from their alternative choices). This implies $S^{\mathrm{v}}(0) = 0.9$. Francey and Garratt emphasized the large scatter in their extracted values for the von Karman constants, assessing mean wind speed errors as the dominant cause; and in an "alternative analysis" of the ITCE, Dyer and Bradley (1982) concluded that the von Karman constants for momentum, heat and water vapour were equal within the limits of uncertainty, with the value 0.40. Summarizing, such measurements as there are suggest that in the inertial sublayer the Schmidt number for water vapour may differ from unity by up to about 10 %, with vapour being transported more efficiently than momentum.

2.1 Schmidt Number Within the RSL

Raupach et al. (1991) define the RSL as "the entire layer dynamically influenced by length scales associated with roughness elements," a deviation of the exchange coefficients from the inertial sublayer form being a salient symptom of that influence (and the most relevant one, in the context of a discussion of the Schmidt number). In the interests of brevity no attempt will be made here to cover all the evidence for a reduced Schmidt number (and Prandtl number) within the RSL, nor the explanations that have been offered. The earliest experimental evidence for a reduced eddy diffusivity dates at least to the 1960s (Lemon et al. 1971) and the inappropriateness of carrying over to small z/z_0 the unadjusted MOST functions (denoted above $\phi_\alpha(\zeta)$, and accommodating a displacement height) was emphasized by Thom et al. (1975). Subsequent field experiments began with work over scrubland (e.g. Garratt 1978) and forest (e.g. Raupach 1979).

The conundrum faced by any attempt to provide a systematic, universal theory of the eddy viscosity/diffusivity near the roughness elements is that, as emphasized earlier, rigorous fluid mechanics (e.g. Finnigan 1985) establishes that the expectation of a universal relationship is naïve: K-theory is unworkable *in principle*. Raupach et al. (1996) emphasize that within the plant canopy itself "the turbulent transfer process is essentially non-local and cannot be described by a local gradient-diffusion relationship," the most dramatic evidence for this being the observation of counter-gradient fluxes (Denmead and Bradley 1985). As Harman and Finnigan (2008) put it "the near-field contribution strongly couples variations in the mean gradients to variations in the source/sink distribution while the far-field contribution dominates the vertical flux. This effective decoupling of fluxes and gradients means that no diffusivity (K) linking vertical flux to vertical gradient locally can be uniquely defined." These statements convey the essential difficulty, which is that a simple flux–gradient relationship characterized by a well-behaved eddy diffusivity need not exist deep within the RSL; and if one will persist in the use of an eddy diffusion treatment then the relationship between eddy diffusivities and the eddy viscosity is unlikely to prove universal. Thus owing to their distinct source distributions, in the RSL different scalars are likely to exhibit differing eddy diffusivities (and Schmidt numbers), which (as noted by Iwata et al. 2010) is problematic for those using a gradient method to determine vertical fluxes.

3 Experiment

The experiment was performed over a uniform field of spring wheat on fair days with suitable winds during 24 July–16 August 2011, at the University of Alberta farm near Saint Albert, Alberta (Fig. 1). The seeding density was 270 plants m^{-2}, the row spacing was 0.25 m and the canopy height varied between about 0.9–0.95 m over the course of the experiment.

A 6 m open-frame, light tubular television tower carried four Climet 0-11B cup anemometers at heights $z_1 \cdots z_4$ = (1.57, 2.55, 3.54, 5.00) m above ground. A Campbell Scientific CSAT3 sonic anemometer and a LI-COR LI-7500A open-path infra-red gas analyzer were operated at height z_2. A LI-COR LI-7000 dual chamber closed-path infra-red gas analyzer, operated in "Reference Estimation Mode," was coupled to air intake lines (Bev-a-line, 1/8 inch internal diameter) at heights z_2, z_3 (or, on two days, at z_1, z_2) via intake switching valves (details below), and determined the mean differences in concentration between the two intake heights.

The sonic anemometer, the open-path gas analyzer and one of the cup anemometers were mounted at the same height $z_2 = 2.55$ m ($\approx h + 1.5$ m). The LI-7500A was offset to leeward of the acoustic paths of the CSAT3, with a separation of 0.15 m and in a configuration that could cause no degradation of wind measurements over the selected range of mean wind directions. The cup anemometer was mounted on a second cross-arm at a distance of about 1.5 m from the CSAT3, such that there could be no wake effect of one on the other for the selected conditions.

The sonic anemometer was aligned with a distant landmark such that wind direction $\beta (= \text{atan} v/u) = 0$ for a westerly wind. For wind directions $|\beta| \leq 45°$ the uniform fetch of wheat field upwind from the instruments exceeded 400 m, and the disturbance at the 400 m range amounted to no worse than an interval of bare ground intervening before a further extension of similar crop. The tall trees visible on Fig. 1 (bearing $\beta = -30°$) were more than 1 km from the instruments (on bearing $\beta = +10°$ an irregular patch of lower trees were closer, at about 600 m). As a criterion for acceptable runs, it was required that the average wind direction satisfy $|\overline{\beta}| \leq 35°$).

Fig. 1 View (telephoto lens) of the instruments and wheat crop, looking towards the south-west. Visible are the cup anemometers, the ultrasonic anemeometer (at height $z = 2.55$ m above ground) and the open-path infra-red gas analyzer (LI-COR LI-7500). Also faintly visible are air lines, taped to a vertical wire and with their intakes coincident with anemometer heights. The LI-7000 analyzer is unseen within the crop. The distance to the north end of the taller trees (see *right* of photo) was 1.04 km and the bearing 240° (i.e. 30° south of west)

3.1 Calibration of the Cup Anemometers Against the Sonic

Selection criteria for acceptable runs included the requirement that $\overline{u}(z_2) \geq 2\,\mathrm{m\,s^{-1}}$ so that there was a negligible possibility of cups having stalled during the measurement. Each anemometer was individually calibrated against the CSAT3, selecting only those periods that were suitable as to exposure and relevance of the wind-speed range. The calibrations were accomplished by periodically switching anemometers such that each spent many hours at the height of the sonic, and correction relations were thereby derived.

3.2 Air Intake Switching and Calibration of Gas Analyzers

The air intake lines were reversed (based on a time signal from the controlling datalogger) so that the measurement cycle was: switch intakes; delay for t_1 to allow equilibration; sample (at 0.5 Hz) for interval t_2; switch intakes. The intake-switching was patterned on Xu et al. (1999). Field intake line lengths were 4.9 m, and air flow rates were controlled at 1.5–2 l/min. On most days the equilibration delay $t_1 = 20$ s (the step response to a change in humidity,

Table 1 Field "zeros"

Date	n	t_{end} (MDT)	t_1 (s)	t_2 (s)	$\overline{\lvert\Delta\overline{\rho}_c\rvert}$ (range) (μmol mol^{-1})	$\overline{\lvert\Delta\overline{\rho}_v\rvert}$ (range) (mmol mol^{-1})
28 July	6	1530	30	60	0.14 ($-0.17 \rightarrow +0.28$)	0.01 ($-0.02 \rightarrow +0.02$)
29 July	5	1300	20	25	0.07 ($-0.12 \rightarrow +0.12$)	0.01 ($-0.03 \rightarrow +0.01$)
1 August	3	2100	20	25	0.29 ($\approx$ const.)	-0.005 ($-0.008 \rightarrow +0.001$)
7 August	4	1730	20	25	0.12 ($\approx$ const.)	0.013 ($0.005 \rightarrow 0.03$)
14 August	4	1230	20	25	0.78 ($\approx$ const.)	0.04 ($0.03 \rightarrow 0.05$)
16 August	3	1030	20	25	1.22 ($0.78 \rightarrow 1.63$)	0.04 ($0.03 \rightarrow 0.04$)

Summary of apparent 30-min concentration differences when (in fact) intakes for the LI-7000 were at same point (intake switching in normal operation). Mean *magnitude* (rounded) of the n recorded 30-min mean concentration differences (in brackets, range of the 30-min means). t_{end} denotes the time (Mountain Daylight Time, MDT) at which the last of the runs with intakes together was completed, while t_1 is the equilibration delay after each polarity switch and t_2 the subsequent duration of sampling. Zeros (but not Schmidt number measurements) were also performed on 14 August. On 16 August the CO_2 zeros during 0900–1030 averaged 0.83 μmol mol^{-1}, but from 1830 to 2000 they averaged 1.62 μmol mol^{-1}; accordingly the S^c measurements of 16 August were discarded for want of confidence in the $\Delta\overline{\rho}_c$ measurements

measured in the laboratory with shorter 2.9 m lines, yielded a time constant of 1.2 s). The sampling period t_2 was normally 25 s.

Two point calibrations of the LI-7500A open-path analyzer (once, prior to field installation) and the closed-path LI-7000 analyzer (21 July, 2 August, 10 August) were performed in the laboratory using three standard gases, viz. "ultra pure" nitrogen (N_2), carbon dioxide in nitrogen at a mixing ratio 364 μmol mol^{-1}, and laboratory air conditioned to a known dewpoint ($T_d = 12.00°$ C) by an LI-610 dewpoint calibrator. Test gases/mixtures were supplied to the analyzers at about 1–1.5 l min^{-1}, either under slight pressurization from the gas cylinders, or by way of the built-in pump on the LI-610; the intake switching system for the LI-7000 was removed during calibrations.

Both analyzers behaved as expected in the laboratory tests. After the first calibration (21 July) the LI-7000 was left running under control of the datalogger and with intake line switching as in the field configuration, but with the intakes placed together in an open flask in the laboratory. Means and standard deviations of the concentration differences were recorded for $N = 31$ half-hour intervals (overnight, the laboratory being unoccupied), using the algorithm employed in the field (see Sect. 3.3). The largest recorded 30-min average concentration differences in H_2O and CO_2 mixing ratios (respectively) were 0.005 mmol mol^{-1} and 0.1 μmol mol^{-1}. The signs of the individual 30-min offsets were random, with the average values being -0.0006 mmol mol^{-1} for H_2O, and 0.03 μmol mol^{-1} for CO_2.

On most field days the profile equipment was operated for several sequential 30-min intervals with the air inlets together, typically at level z_1 but also (on one occasion) in a flask at the base of the wheat canopy. As the polarity switching was in normal operation for these tests, the values of the 30-min mean concentration differences (which will be designated $\Delta\overline{\rho}_c$ and $\Delta\overline{\rho}_v$ for carbon dioxide and water vapour, respectively) would ideally have been negligible. In fact these offsets were larger than they had been in the laboratory (see Table 1), and on some occasions (for CO_2 in particular) did not appear to be random,[2] although the hazard of having only a handful of estimates is that one may easily err in suspecting a bias

[2] Might these offsets reflect a temporal trend in CO_2 concentration, in combination with the delay $(t_1 + t_2)$ between samples in the two intake polarities? A (large) trend of order 10 μmol mol^{-1} h^{-1}, coupled with $t_1 + t_2 = 45$ s, would produce an offset $\Delta\rho_c \sim 0.1$ μmol mol^{-1}, i.e. too small to explain the observed values.

Table 2 Statistics of runs accepted for analysis (criteria: intakes at (z_2, z_3), $|\overline{\beta}| \leq 35^{\circ}$, $\overline{u}(z_2) \geq 2.0\,\mathrm{m\,s^{-1}}$)

Date	n	$\overline{u}(z_2)$ (m s^{-1})	β (°)	Q_E (W m^{-2})	Bowen ratio	$-F_c$ (mg m^{-2} s^{-1})	CPP (mm)
28 July	3	2.22 (.04)	31 (2)	256 (100)	0.11 (.07)	1.19 (.13)	1
29 July	6	2.70 (.46)	2 (30)	262 (55)	0.19 (.07)	0.96 (.22)	.5
1 August	19	3.43 (.58)	−3 (11)	347 (85)	0.11 (.12)	1.07 (.27)	6
7 August	11	3.37 (.37)	−18 (9)	225 (56)	0.36 (.13)	0.96 (.20)	13.5
16 August	15	3.09 (.38)	3 (10)	267 (46)	0.37 (.10)	0.53 (.12)	0

Daily mean-of-means (and standard deviation, in brackets) of the n acceptable 30-min mean runs of the given day. CPP is the cumulative prior precipitation (measured at Edmonton Namao, 11 km from the field site) over the five previous days (i.e. excluding the measurement day). As rain was on most occasions convective in origin, the smaller values of CPP (including zero) recorded at Namao do not necessarily represent the truth of events at the field site at St. Albert

(i.e. systematic, rather than random, error). On every occasion these "field zeros" were more satisfactory (i.e. smaller in relation to the "true" differences measured when the intakes were separated) for water vapour than for carbon dioxide. Based on Table 1 bias corrections were applied to the CO_2 differences on August 1 and August 7, while the CO_2 measurements of August 16 were discarded (Table 2).

3.3 Data Acquisition

All signals except those from the Climet cup anemometers were acquired by a Campbell Scientific CR3000 datalogger. The CSAT3 and LI-7500A signals were sampled at 10 Hz using the "SDM" mode (digital signals), whereas conveniently scaled analog signals from the LI-7000 were sampled using single-ended voltage inputs on a ±5,000 mV range. The humidity and CO_2 signals from the LI-7500A (ρ_v, ρ_c) were synchronized with the velocity signals from the CSAT3: a single 100 ms delay of the anemometer signals was performed in software, and added to the built-in two scan pipeline delay implied a total delay of 300 ms. A parameter of the LI-7500A was set so as to achieve a closely matched delay (297.7 ms). The digital LI-7500A signals ρ_c and ρ_v were delivered to the logger in mg m^{-3} and g m^{-3} respectively, and a constant (600) was subtracted from ρ_c to reduce round-off errors in the logger calculations.

The air intake line switching and the sampling of the slow (LI-7000) analyzer were coordinated by a second program table in the CR3000 with scan interval 0.5 s. Distinct accumulators for each polarity, viz. $\Delta\rho_c^{(+)}$, $\Delta\rho_c^{(-)}$, $\Delta\rho_v^{(+)}$, $\Delta\rho_v^{(-)}$, were loaded with *zeros* upon each scan during the equilibration interval t_1 and upon each scan during the sampling interval t_2 for which polarity was "wrong." At the end of the 30-min run the logger stored the averages $\overline{\Delta\rho_c}^{(+)}$, $\overline{\Delta\rho_c}^{(-)}$, $\overline{\Delta\rho_v}^{(+)}$, $\overline{\Delta\rho_c}^{(-)}$ and the mean vertical concentration differences were subsequently computed as (e.g.)

$$\Delta\overline{\rho}_v = \frac{2(t_1 + t_2)}{t_2} \frac{\overline{\Delta\rho_v}^{(+)} - \overline{\Delta\rho_v}^{(-)}}{2}. \tag{6}$$

The scaling factor $2(t_1 + t_2)/t_2$ corrects for the fact that the accumulator for (e.g.) $\overline{\Delta\rho_c}^{(+)}$ sampled its signal only for a duration t_2 within each interval $2(t_1 + t_2)$, while being loaded with zeros for the balance $2t_1 + t_2$ of the wait-sample-wait-sample cycle.

3.4 Eddy-Flux Computations and Corrections

The Reynolds stress tensor and scalar fluxes (etc.) were computed offline. A double coordinate rotation enforced $\overline{v} = 0$ then $\overline{w} = 0$ (e.g. Wilczak et al. 2001), and cited variables are "post-rotation." The friction velocity was computed as

$$u_*^4 = \overline{u'w'}^2 + \overline{v'w'}^2, \tag{7}$$

which is the most suitable definition under the paradigm (Eq. 15) of a vertical flux of "horizontal" momentum being "driven" by a vertical gradient in mean horizontal wind speed. The Obukhov length was computed as

$$L = \frac{-u_*^3 T_{v0}}{\kappa g Q} \tag{8}$$

where κ (evaluated as 0.4) is the von Karman constant for momentum, and T_{v0} and Q are respectively the mean virtual temperature (in kelvin) and the (kinematic) virtual heat flux density. The latter are given by

$$T_{v0} = T_0 \left(1 + \mu q_0\right), \tag{9}$$

$$Q = \overline{w'T'} + \mu T_0 \overline{w'q'}, \tag{10}$$

where T_0 and q_0 are the mean temperature (in kelvin) and mean specific humidity; $\mu = \varepsilon^{-1} + 1 \approx 0.61$, where ε is the ratio $\varepsilon = m_v/m_d = 0.622$ of the molar masses of water vapour and dry air; and (as earlier) $q \equiv \rho_v/\rho_0$ is the specific humidity, ρ_0 being mean air density.

As the CSAT3 "sonic temperature" (T_s) was used to compute the sensible heat flux, and in view of the large evaporative fluxes experienced, the Schotanus et al. (1983) correction

$$\overline{w'T'} = \overline{w'T_s'} - bT_0\overline{w'q'} \tag{11}$$

was significant ($b = 0.32/\varepsilon \approx 0.51$). Not uncommonly in these measurements at late afternoon the corrected sensible heat flux remained positive (unstable stratification) even though the "raw" post-rotation sensible heat flux had turned negative. The Webb et al. (1980) corrections, in the terminology used here, are:

$$F_c = \overline{w'\rho_c'} + \mu\frac{\overline{\rho}_c}{\rho_0}\overline{w'\rho_v'} + (1 + \mu\sigma)\frac{\overline{\rho}_c}{T_0}\overline{w'T'}, \tag{12}$$

$$F_v = \left(1 + \varepsilon^{-1}\sigma\right)\left(\overline{w'\rho_v'} + \frac{\overline{\rho}_v}{T_0}\overline{w'T'}\right), \tag{13}$$

where $\sigma = \overline{\rho}_v/\rho_0$. These interlinked corrections (entailing Eqs. 11–13) were accomplished by an iteration that continued until the percentage changes in the fluxes (on the final pass) were all smaller than 10^{-4}.

Finally, the vertical fluxes of water vapour and carbon dioxide were boosted by 6 % to compensate for flux loss due to the 0.15-m separation between the fast-response infrared gas analyzer and the acoustic path of the sonic anemometer. This theoretical correction factor was arrived at by computing Moore's (1986; Eq. 11) transfer function and its filtering effect on the the idealized cospectrum of Kaimal et al. (1972, Eq. 21f; see also Kaimal and Finnigan 1994, Eq. 2.57), adjusted to account for the displacement height (the sonic path-length correction proved negligible). The computed sonic—gas-analyzer separation correction was constant

to two significant figures over the wind-speed range of interest. The result of this correction was to *decrease* the Schmidt numbers by 6 %.[3]

3.5 Computation of the Schmidt Number

The experiment and the data analysis are predicated on an assumption that relevant mean vertical fluxes are height independent. Let $\Delta\overline{q}_{21} = \overline{q}(z_2) - \overline{q}(z_1)$ be the difference in mean specific humidity between two heights z_1, z_2 (where $z_1 < z_2$) and let $\Delta\overline{u}_{21} = \overline{u}(z_2) - \overline{u}(z_1)$ be the difference in mean wind speed between the same two heights. By invoking the gradient-diffusion paradigm the mean humidity difference may be related to the Schmidt number, viz.

$$\begin{aligned}
\Delta\overline{q}_{21} \equiv \overline{q}(z_2) - \overline{q}(z_1) &= \int_{z_1}^{z_2} \frac{\partial \overline{q}}{\partial z} \mathrm{d}z \\
&= \int_{z_1}^{z_2} \frac{-\overline{w'q'}}{K_{\mathrm{v}}(z)} \mathrm{d}z \\
&= -\overline{w'q'} \int_{z_1}^{z_2} \frac{\mathrm{d}z}{K_{\mathrm{v}}(z)} \\
&= -\overline{w'q'} \int_{z_1}^{z_2} \frac{S^{\mathrm{v}} \mathrm{d}z}{K(z)} \\
&= -S^{\mathrm{v}} \overline{w'q'} \int_{z_1}^{z_2} \frac{\mathrm{d}z}{K(z)},
\end{aligned} \tag{14}$$

where it has been assumed that the eddy diffusivity K_{v} for vapour is related to the eddy viscosity K as $K_{\mathrm{v}} = K/S^{\mathrm{v}}$, with S^{v} *independent of height* over the height interval. Similarly

$$\Delta\overline{u}_{21} \equiv \overline{u}(z_2) - \overline{u}(z_1) = \int_{z_1}^{z_2} \frac{\partial \overline{u}}{\partial z} \mathrm{d}z = u_*^2 \int_{z_1}^{z_2} \frac{\mathrm{d}z}{K(z)}. \tag{15}$$

Thus,

$$\Delta\overline{q}_{21} = -S^{\mathrm{v}} \overline{w'q'} \frac{\Delta\overline{u}_{21}}{u_*^2} \tag{16}$$

or

$$S^{\mathrm{v}} = -\frac{\Delta\overline{q}_{21}}{\overline{w'q'}} \frac{u_*^2}{\Delta\overline{u}_{21}} = \frac{\Delta\overline{q}_{21}}{q_*} \frac{u_*}{\Delta\overline{u}_{21}}. \tag{17}$$

An analogous formulation holds for the Schmidt number S^{c} for carbon dioxide. The particular choice for the intake levels z_1, z_2 makes no *numerical* entry into Eq. 17, and neither does the canopy height h. However a meaningful interpretation of a measured Schmidt number demands that the underlying observations be in the far field of relevant sources and sinks.

[3] To better than 1 %, computed fluxes and Schmidt numbers were indifferent to whether this correction was applied before or after the WPL correction.

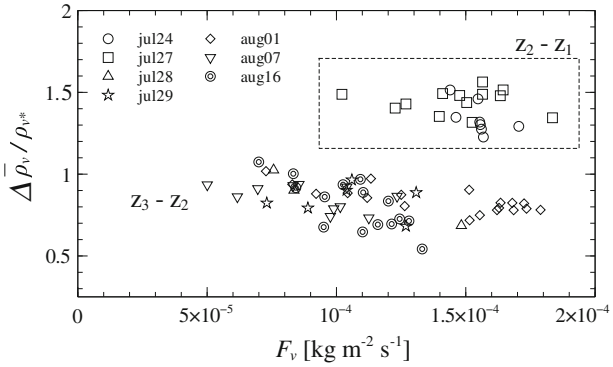

Fig. 2 Normalized mean absolute humidity differences versus the corresponding vapour flux. Selection: $|\beta| \leq 35°$, $\overline{u}(z_2) \geq 2\,\mathrm{m\,s^{-1}}$

3.6 Assessment of Confidence Intervals

The needed difference "$\Delta\overline{u}_{21}$" in mean wind speed was computed as a small difference (over the duration of these measurements typically of order 0.5 and never greater than $0.8\,\mathrm{m\,s^{-1}}$) between two relatively large absolute wind speeds. Accordingly the absolute uncertainty in $\Delta\overline{u}_{21}$ is twice one's realistic assessment of the absolute uncertainty of the Climet anemometers (taken as $0.03\,\mathrm{m\,s^{-1}}$) and this results in rather a large *fractional* uncertainty in $\Delta\overline{u}_{21}$ of something like 0.06/0.6, i.e. around 10 %. In hindsight this is one of the weaknesses of the experimental design, albeit a difficult one to circumvent. On the other hand the accuracy of wind-speed measurements has no bearing on one's deduction of the *ratio* $S^{\mathrm{c}}/S^{\mathrm{v}}$ of the Schmidt numbers for carbon dioxide and water vapour.

As stated earlier, measured differences in CO_2 concentration were adjusted by removing the apparent bias (see Table 1) on 1 August and after; no such adjustments were made for the humidity differences. The absolute uncertainties for the CO_2 and water vapour differences were taken (on the basis of Table 1) to be $0.15\,\mu\mathrm{mol\,mol^{-1}}$ and $0.02\,\mathrm{mmol\,mol^{-1}}$. Uncertainty bars on diagrams to follow were computed by adding the fractional uncertainties stemming from the wind-speed and concentration differences to obtain the fractional uncertainty in the Schmidt number. The span of the error bar is (twice) the corresponding absolute uncertainty.

4 Results

From nearly neutral wind profiles ($|L| \geq 200$ m) the displacement length for the wheat canopy was estimated as $d = 0.56$ m. Figure 2 displays the normalized mean humidity differences $\Delta\overline{\rho}_{\mathrm{v}}/\rho_{\mathrm{v}*}$ as a function of the evaporative flux density F_{v} (where $\rho_{\mathrm{v}*} \equiv -F_{\mathrm{v}}/u_*$ is the absolute humidity fluctuation scaling parameter). Even for a fixed pair of levels (note: $z_3 - z_2 \approx z_2 - z_1$) this dimensionless property is not expected to be constant, but it should be roughly insensitive to overall wind speed and the magnitude of the scalar flux. For both species the normalized humidity differences between the upper two intake levels were smaller than between the lower two levels, which is consistent with the prediction of MOST that, for a sufficiently small height increment Δz about height z, the normalized difference in mean absolute humidity

$$\frac{\Delta\overline{\rho}_{\mathrm{v}}}{\rho_{\mathrm{v}*}} \approx \frac{\Delta z}{k_{\mathrm{v}}(z-d)}\phi_{\mathrm{v}}\left(\frac{z-d}{L}\right) \tag{18}$$

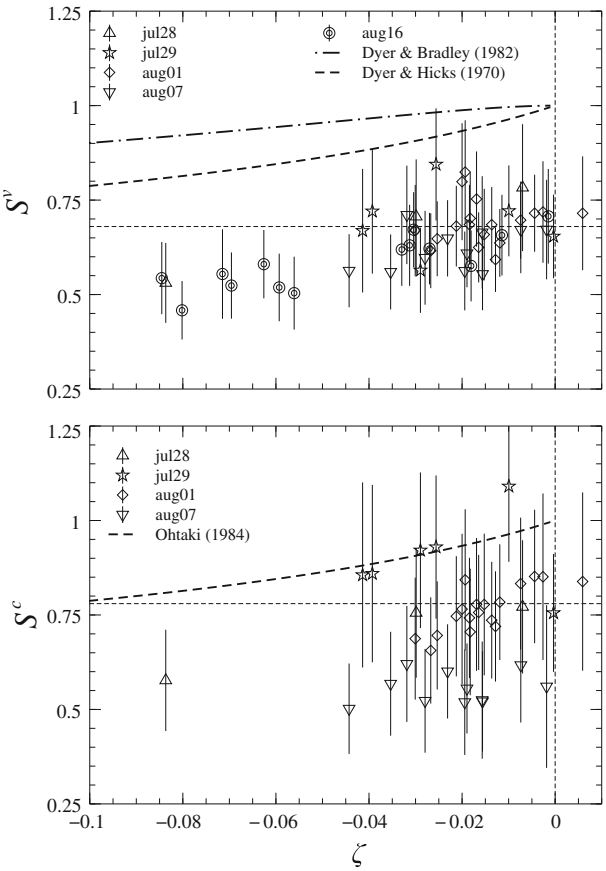

Fig. 3 S^v and S^c versus $\zeta = (z-d)/L$ for data with intakes at levels z_2, z_3 (2.55 m and 3.54 m). Selection: $|\beta| \leq 35°$, $\overline{u}(z_2) \geq 2\,\mathrm{m\,s^{-1}}$. The *horizontal dashed lines* designate $S^v = 0.68$, $S^c = 0.78$. The *error bars* denote ± the uncertainty (see Sect. 3.6)

must decrease with increasing $z-d$ (here ϕ_v is the MOST function for the mean humidity gradient).

Figure 3 plots all measured Schmidt numbers derived with the intakes at levels z_2, z_3 versus $(z-d)/L$ (taking $z = \sqrt{z_2 z_3}$). Both S^v and S^c decrease with increasing thermal instability, and most often $S^v < S^c$. The average values and standard deviations over intervals for which $L \leq -150$ m were $S^v(0) = 0.68$ ($n = 14$, standard deviation 0.05) and $S^c(0) = 0.78$ ($n = 12$, standard deviation 0.13). If the small bias corrections of Table 1 are used to adjust $\Delta\overline{\rho}_v$, the average Schmidt number for water vapour decreases slightly to $S^v(0) = 0.67$ (standard deviation 0.06). If the acceptable mean wind direction range is reduced to $|\overline{\beta}| \leq 20°$ the patterns do not change: $S^v(0) = 0.67$ ($n = 11$) and $S^v(0) = 0.76$ ($n = 9$).

Also plotted on Fig. 3 are empirical relations for S^v, S^c based on the Monin–Obukhov functions (for unstable stratification) reported from earlier analyses of the flux–gradient relationship, either over extensive grassland or over a crop. For S^v it follows from Dyer and Bradley (1982) that for the measurements of ITCE76

$$S^v = \frac{\phi_v}{\phi_m} = \frac{(1-14\zeta)^{-1/2}}{(1-28\zeta)^{-1/4}}, \tag{19}$$

while from Dyer and Hicks (1970)

$$S^{\mathrm{v}} = (1 - 16\zeta)^{-1/4}\,. \tag{20}$$

As for CO_2, from measurements (presumably in the RSL) at heights $z/h = (1.2, 1.9)$ over a rice paddy of height $h = 0.9$ m Ohtaki (1980) inferred that the universal functions for the dimensionless mean wind shear and the mean CO_2 concentration gradient were

$$\begin{aligned} \phi_{\mathrm{m}}(\zeta) &= (1 - 15\zeta)^{-1/4}\,, \\ \phi_{\mathrm{c}}(\zeta) &= 0.92 + 13.8\zeta, \end{aligned} \tag{21}$$

implying $S^{\mathrm{c}}(0) = 0.92$; however based on the strength of further similar measurements Ohtaki (1984) found $\phi_{\mathrm{c}} = (1 - 16\zeta)^{-1/2}$, which in combination with the Businger–Dyer form $\phi_{\mathrm{m}} = (1 - 16\zeta)^{-1/4}$) implies

$$S^{\mathrm{c}} = (1 - 16\zeta)^{-1/4}\,. \tag{22}$$

5 Conclusion

From Fig. 3 it is clear that, almost without exception, these observed Schmidt numbers fall well below what is considered the norm for an inertial sublayer. The straightforward interpretation is that the depth of the RSL extended into or above the layer ($2.55 \leq z \leq 3.54$ m) sampled by the instruments, which is compatible with generic estimates of 2–3h for the RSL depth (e.g. Kaimal and Finnigan 1994; Foken 2006).

Turning to the relative magnitudes of S^{v} and S^{c}, in the majority of cases $S^{\mathrm{v}}/S^{\mathrm{c}} < 1$. This is not necessarily surprising, as the Lagrangian viewpoint on dispersion certainly permits differing eddy diffusivities for different scalars. A reviewer wondered whether the mean source height for water vapour was farther below the instruments than the mean sink height for carbon dioxide (implying $S^{\mathrm{v}} < S^{\mathrm{c}}$, because the eddy diffusivity must always increase with increasing distance above the source). That possibility cannot be discounted, and stimulated contemplation as to whether during such-and-such a run the canopy might have been damp after rain, and of the role of changing cloud cover in regard to the height profile of the assimilation rate. However none of the quantities measured in this experiment was found to relate consistently[4] with $S^{\mathrm{v}}/S^{\mathrm{c}}$.

Acknowledgments This work has been supported by the Natural Sciences and Engineering Research Council of Canada. Peter Carlson (Earth & Atmospheric Sciences, University of Alberta) helped with design of the air intake switching apparatus. The author is grateful to three unknown reviewers who provided incisive and constructive suggestions.

References

Arya SP (2001) Introduction to micrometeorology, Second edition. Academic Press, New York, 420 pp
De Ridder K (2010) Bulk transfer relations for the roughness sublayer. Boundary-Layer Meteorol 134:257–267
Delaunay D (1996) Numerical simulation of atmospheric dispersion in an urban site: comparison with field data. J Wind Eng Ind Aerodyn 64:221–231

[4] It is pertinent to recall the rather uncertain bias correction for the $\Delta\overline{\rho}_{\mathrm{c}}$ measurements underlying S^{c}: no plausible assumption regarding that bias yielded a tidy pattern for $S^{\mathrm{v}}/S^{\mathrm{c}}$.

Denmead O, Bradley E (1985) Flux–gradient relationships in a forest canopy. In: Hutchison B, Hicks B (eds) The forest–atmosphere interaction. D. Reidel Pub. Co., Boston (pp 421–442), 708 pp
Dyer A (1974) A review of flux-profile relationships. Boundary-Layer Meteorol 7:363–372
Dyer A, Bradley E (1982) An alternative analysis of flux–gradient relationships at the 1976 ITCE. Boundary-Layer Meteorol 22:3–19
Dyer A, Hicks B (1970) Flux–gradient relationships in the constant flux layer. Q J R Meteorol Soc 96:715–721
Finnigan J (1985) Turbulent transport in flexible plant canopies. In: Hutchison B, Hicks B (eds) The forest–atmosphere interaction. D. Reidel Pub. Co., Boston, pp 443–480
Foken T (2006) 50 years of the Monin–Obukhov similarity theory. Boundary-Layer Meteorol 119:431–447
Francey R, Garratt JR (1981) Interpretation of flux-profile observations at ITCE (1976). J Appl Meteorol 20:603–618
Garratt JR (1978) Flux profile relations above tall vegetation. Q J R Meteorol Soc 104:199–211
Glenn A, Amiro B, Tenuta M, Stewart S, Wagner-Riddle C (2010) Carbon dioxide exchange in a northern Prairie cropping system over three years. Agric For Meteorol 150:908–918
Harman I, Finnigan J (2008) Scalar concentration profiles in the canopy and roughness sublayer. Boundary-Layer Meteorol 129:323–351
Hassid S (1983) Turbulent Schmidt number for diffusion models in the neutral boundary layer. Atmos Environ 17:523–527
Huq P, Stewart E (2008) Measurements and analysis of the turbulent Schmidt number in density stratified turbulence. Geophys Res Lett 35:L23604. doi:10.1029/2008GL036056
Iwata H, Harazono Y, Ueyama M (2010) Influence of source/sink distributions on flux–gradient relationships in the roughness sublayer over an open forest canopy under unstable conditions. Boundary-Layer Meteorol 136:391–405
Kaimal J, Finnigan J (1994) Atmospheric boundary layer flows. Oxford University Press, Oxford, 289 pp
Kaimal J, Wyngaard J, Izumi Y, Coté O (1972) Spectral characteristics of surface-layer turbulence. Q J R Meteorol Soc 98:563–589
Lemon E, Stewart D, Shawcroft R (1971) The sun's work in a cornfield. Science 174:371–378
Moore C (1986) Frequency response corrections for eddy correlation systems. Boundary-Layer Meteorol 37:17–36
Ohtaki E (1980) Turbulent transport of carbon dioxide over a paddy field. Boundary-Layer Meteorol 19:315–336
Ohtaki E (1984) The budget of carbon dioxide variance in the surface layer over vegetated fields. Boundary-Layer Meteorol 29:251–261
Pruitt W, Morgan D, Lourence F (1973) Momentum and mass transfers in the surface boundary layer. Q J R Meteorol Soc 99:370–386
Raupach MR (1979) Anomalies in flux–gradient relationships over forest. Boundary-Layer Meteorol 16:467–486
Raupach M (1987) A Lagrangian analysis of scalar transfer in vegetation canopies. Q J R Meteorol Soc 113:107–120
Raupach M, Antonia R, Rajagopalan S (1991) Rough-wall turbulent boundary layers. Appl Mech Rev 44:1–25
Raupach M, Finnigan J, Brunet Y (1996) Coherent eddies and turbulence in vegetation canopies: the mixing layer analogy. Boundary-Layer Meteorol 78:351–382
Sawford BL (2001) Project Prairie Grass—a classic atmospheric dispersion experiment revisited. In: 14th Australian fluid mechanics conference, Adelaide
Schotanus P, Nieuwstadt FTM, DeBruin HAR (1983) Temperature measurement with a sonic anemometer and its application to heat and moisture fluctuations. Boundary-Layer Meteorol 26:81–93
Taylor G (1921) Diffusion by Continuous Movements. Proc Lond Math Soc Ser 2 A20:196–211
Thom A, Stewart J, Oliver H, Gash J (1975) Comparison of aerodynamic and energy budget estimates of fluxes over a pine forest. Q J R Meteorol Soc 101:93–105
Tominaga Y, Stathopoulos T (2007) Turbulent Schmidt numbers for CFD analysis with various types of flowfield. Atmos Environ 41:8091–8099
Webb EK, Pearman GI, Leuning R (1980) Correction of flux measurements for density effects due to heat and water vapour transfer. Q J R Meteorol Soc 106:85–100
Wilczak J, Oncley S, Stage S (2001) Sonic anemometer tilt correction algorithms. Boundary-Layer Meteorol 99:127–150
Wilson J (1982) Turbulent dispersion in the atmospheric surface-layer. Boundary-Layer Meteorol 22:399–420
Wilson J (1989) Turbulent transport within the plant canopy. In: Estimation of areal evapotranspiration. International Association of Hydrological Sciences, Gothenburg, pp 43–80
Wilson J, Yee E (2007) A critical examination of the random displacement model of turbulent dispersion. Boundary-Layer Meteorol 125:399–416

Wilson J, Clarkson T, Hadfield M (1984) Observations of wind flow and tracer-gas dispersion over sand dunes. N Z J Sci 27:237–242

Xu L, Matista A, Hsiao T (1999) A technique for measuring CO_2 and water vapor profiles within and above plant canopies over short periods. Agric For Meteorol 94:1–12